Accepted Manuscript

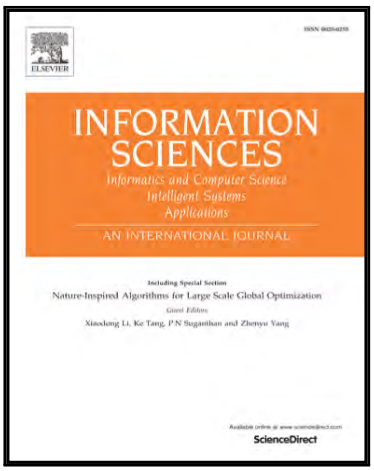

Event-triggered Predictor-based Control with Gain-Scheduling and Extended State Observer for Networked Control Systems

Antonio González, Angel Cuenca, Vicente Balaguer, Pedro García

PII: S0020-0255(19)30292-0
DOI: https://doi.org/10.1016/j.ins.2019.03.081
Reference: INS 14421

To appear in: *Information Sciences*

Received date: 14 December 2018
Revised date: 29 January 2019
Accepted date: 31 March 2019

Please cite this article as: Antonio González, Angel Cuenca, Vicente Balaguer, Pedro García, Event-triggered Predictor-based Control with Gain-Scheduling and Extended State Observer for Networked Control Systems, *Information Sciences* (2019), doi: https://doi.org/10.1016/j.ins.2019.03.081

Highlights

- A novel control scheme is presented for Networked Control Systems.
- We combine Event-triggered control with Predictor-feedback approaches, Gain-Scheduling, and Extended State Observer.
- Time-varying delays, together with packet loss, packet disorder and mismatched disturbances are effectively counteracted.
- A CCL-based controller design algorithm is provided to improve closedloop performance.
- The proposed control method is experimentally validated in a quadrotor platform.

Event-triggered Predictor-based Control with Gain-Scheduling and Extended State Observer for Networked Control Systems[☆]

Antonio González, Angel Cuenca, Vicente Balaguer, Pedro García

Abstract

This paper investigates the stabilization of Networked Control Systems (NCS) with mismatched disturbances through a novel Event-Triggered Control (ETC), composed of a predictor-feedback scheme and a gain-scheduled Extended State Observer (ESO). The key idea of the proposed control strategy is threefold: i) to reduce resource usage in the NCS (bandwidth, energy) while maintaining a satisfactory control performance; ii) to counteract the main negative effects of NCS: time-varying delays, packet dropouts, packet disorder, and (iii) to reject the steady-state error in the controlled output due to mismatched disturbances. Moreover, we address the co-design of the controller/observer gains, together with the event-triggered parameters, by means of Linear Matrix Inequalities (LMI) and Cone Complementarity Linearization (CCL) approaches. Finally, we illustrate the effectiveness of the proposed control synthesis by simulation and experimental results in a Unmanned Aerial Vehicle (UAV) based test-bed platform.

Keywords: Time-varying delay, Networked Control System, Packet disorder, Packet loss, Predictor-based control, Gain-Scheduling, ESO

[☆]a) This manuscript is the authors' original work and has not been published nor has it been submitted simultaneously elsewhere. b) All authors have checked the manuscript and have agreed to the submission. The corresponding author is A. Gonzalez. He is with the Instituto de Investigación en Ingeniería de Aragón, Universidad de Zaragoza C/María de Luna 1, E50018 Zaragoza (Spain) (e-mail: angonsor@unizar.es). A. Cuenca, V. Balaguer and P. Garcia are with the Departamento de Ingeniería de Sistemas y Automática (DISA), Instituto Universitario de Automática e Informática Industrial (AI2), Universitat Politècnica de València (UPV)(e-mails: acuenca@isa.upv.es, vibagar3@etsii.upv.es, pggil@isa.upv.es)

1. Introduction

Networked Control Systems (NCS) are characterized by the fact that the control loop is closed over a real-time communication network, and therefore the components, i.e., controllers, sensors and actuators are spatially distributed and connected [40]. The first works on NCS date from the last decade of the previous century [16, 32, 21]. Since then, it has become a prolific area (see for example in [15] and [39], where a general idea about NCS is presented). Sharing a communication network implies well-known advantages: low installation and maintenance costs, high reliability, increased system flexibility, and decreased wiring and weight. However, NCS also lead to some undesirable phenomena, which may cause poor performance or even instability if they are not taken into account during the control design. A recent survey that describes a general framework for analysis and control synthesis of NCS can be found in [40] and references therein.

In this paper we will consider, together with the presence of mismatched disturbances, the following network effects: time-varying communications delays, packet dropouts, packet disorder and bandwidth constraints. Such phenomena have been extensively investigated in the literature. For instance, the effect of time-varying delays has been tackled under different control schemes: via state-feedback control [4], multi-rate control [33], state estimators [26], [30], and reset-based control in [2], [31]. Packet dropouts have been faced using predictive control [20], predictor-observer methods [5, 8], gain scheduling [9], etc. Packet disordering has also been investigated in [22, 23, 37] by introducing different packet reordering mechanisms, and in [33, 7, 6] by using dual-rate control.

In event-triggered control (ETC) [19, 18], data packets are transmitted only when event-based conditions are satisfied. Compared to the traditional time-triggered control, ETC enables to further reduce resource utilization, such as bandwidth and energy consumption [28, 8]. Indeed, the design of more efficient ETC strategies is a matter of current research, with interesting applications related to the field of NCS: containment control of multiagent systems [44], leader-following consensus [45] and distributed formation control [12], among others. As the controller is provided with less system data, event-based state prediction techniques must be additionally included in order to estimate the not available data and keep performance properties. An ETC scenario can be developed in both continuous-time (see [19], and references therein) and discrete-time frameworks (see [27] among others).

On another line of research, time delay compensation techniques (or dead-time compensator (DTC) schemes) have been widely implemented in control systems with input/output delay to improve the closed-loop performance of classical controllers ([29, 13]). The underlying idea behind DTC consists in obtaining a future prediction of the system state in order to find an equivalent delay-free closed-loop system model, simplifying the control design. Nevertheless, this feature can only be achieved if delays are known in advance and time-constant. In the presence of time-varying delay mismatches, the closed-loop performance may be sharply degraded or even unstable if delay intervals are sufficiently large. This fact may impose severe limitations on the applicability of predictor-like techniques on NCS, where time delays are frequently subject to time-variations, and other phenomena, such as packet dropouts and packet disorder, may occur. The stability analysis of NCS using time delay compensation techniques has been investigated [41, 38, 42].

It is worth mentioning that the existing error between the exact and the approximated predictions in a disturbed system cannot be removed, even in case of time-constant disturbances using integral action [34]. To overcome this limitation, predictor-feedback approaches were recently combined with Extended State Observer (ESO) to actively reject external disturbances in the presence of time-constant delays [25, 17], and further extended to time-varying delays [14]. These last works considered disturbances that affect the state through channels in which the input has no direct influence (mismatched disturbances), which are generally more difficult to handle for disturbance rejection purposes [3]. It is worthwhile mentioning that a complete disturbance rejection is only achievable if the dynamics of the disturbance component is known in advance. In such case, the disturbance signal can be observed by an ESO in order to further cancel its steady-state effect in the controlled output.

However, to the best authors' knowledge, the control synthesis of event-triggered predictor-feedback control with ESO to face time-varying delays, packet loss, packet disorder, bandwidth constraints and mismatched disturbances in a single framework, has not been fully investigated.

In this paper, a novel event-triggered control strategy for NCS consisting of a predictor-based control with a delay-dependent gain-scheduled ESO is proposed, where the provided gain-scheduling method is used to counteract the effect of the resulting time-varying delays due to transmission delays, packet dropouts and packet disorders. In addition, the following key aspects have been taken into account:

- (i) The NCS under consideration contemplates the existence of two independent links (from sensor to controller (SC), and from controller to actuator (CA)).
- (ii) The negative effect of mismatched disturbances, along with time-varying delays, packet dropouts and packet disorder in the sensor-to-controller link are counteracted by a properly designed gain-scheduled ESO [14].
- (iii) Time-varying delays, packet dropouts and packet disorder in the controller-to-actuator link are partially compensated by the Artstein's reduction method [1].
- (iv) An event-triggered mechanism is implemented to reduce the number of data packets to be transmitted in both links. The design of the control and observer gains, together with the event-triggered parameters, are carried out by Cone Complementarity Linearization (CCL) algorithm [10] to improve the closed-loop performance.

The paper is structured as follows. In Section 2, the problem is described and some assumptions and preliminaries are introduced. In Section 3, the proposed control structure is presented. Section 4 presents the stability analysis for the considered NCS. Section 5 presents the control synthesis algorithm. In section 6, simulation examples are presented. In section 7, the control solution is experimentally validated using a UAV-based platform. Finally, some conclusions and perspectives are outlined in Section 8.

2. Problem statement

Consider the NCS depicted in Figure 1, where the plant is described by the following discrete-time system model:

$$\begin{cases} x_{k+1} = Ax_k + Bu_{k-d_k^{CA}} + Fw_k, \\ y_k = Cx_k, \qquad y_{s,k} = C_s x_k, \end{cases} \tag{1}$$

where $A \in \mathcal{R}^{n\times n}$, $B \in \mathcal{R}^{n\times m}$, $F \in \mathcal{R}^{n\times q}$, $C \in \mathcal{R}^{p\times n}$ and $C_s \in \mathcal{R}^{p_s\times n}$ are the system matrices, $x_k \in \mathcal{R}^n$ is the system state, $u_{k-d_k^{CA}} \in \mathcal{R}^m$ is the *delayed* control action, $w_k \in \mathcal{R}^q$ is an unknown external disturbance, $y_k \in \mathcal{R}^p$ is the measured output, and $y_{s,k} \in \mathcal{R}^{p_s}$ is the controlled output. Also, consider the

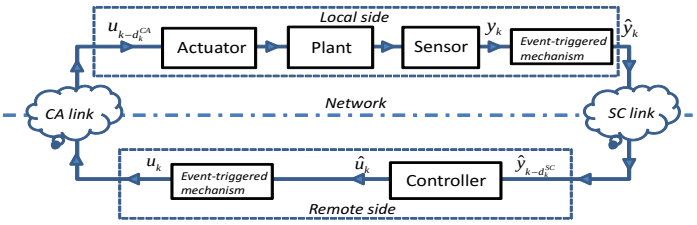

Figure 1: Block-diagram of the NCS

output feedback controller $u_k = \mathcal{F}_u\left(y_{k-d_k^{SC}}\right)$, where $\mathcal{F}_u(.) : \mathcal{R}^p \to \mathcal{R}^m$ is the control scheme to be designed, and $y_{k-d_k^{SC}}$ is the *delayed* measured output system.

The sensor and the actuator are both located closed to the plant, and they interact with the remotely located controller through the sensor-to-controller link (SC) for exchanging measurement data, and through the controller-to-actuator (CA) link for exchanging control actions, respectively.

Let us consider the following assumptions:

Assumption 1. *The controller is digitally implemented with sampling period T_s, and the control actions are applied at the instants in which the packets containing them are received, following a Zero Order Hold (ZOH) method.*

Assumption 2. *A buffer operatively connected to the corresponding interface for storing each received data packet is available in both sides (remote and local). In this way, when data packets are lost, the last received one is processed.*

Assumption 3. *The input and output delays d_k^{CA}, d_k^{SC} are assumed to be unknown time-varying, and satisfy:*

$$\begin{aligned} h_1^{CA} \leq d_k^{CA} \leq h_2^{CA}, \\ h_1^{SC} \leq d_k^{SC} \leq h_2^{SC}, \end{aligned} \tag{2}$$

where each pair (h_1^{CA}, h_2^{CA}) and (h_1^{SC}, h_2^{SC}) are known.

Assumption 4. *[36] The external disturbance $w_k \in \mathcal{R}^q$ in (1) can be modeled as $w_k = \omega_{u,k} + \omega_k$, where $\omega_{u,k} \in \mathcal{L}_2[0,\infty)$ is a completely unknown*

bounded signal that represents the unmodeled disturbance components, and ω_k *is a disturbance component represented by the exogenous system:*

$$\chi_{k+1} = A_w \chi_k, \qquad \omega_k = C_w \chi_k \tag{3}$$

where $\chi_k \in \mathcal{R}^r$ *is the generator vector with unknown initial condition* χ_0*, and* $A_w \in \mathcal{R}^r$*,* $C_w \in \mathcal{R}^{q \times r}$ *are known matrices (the so-called exogenous system), where the spectral radius of* A_w *is less or equal to* 1*.*

Assumption 5. *There exist* $K \in \mathcal{R}^{m \times n}$ *and* $\mathcal{L} \in \mathcal{R}^{(n+q) \times p}$ *such that the matrices* $(A + BK)$ *and* $(\mathcal{A} - \mathcal{L}\mathcal{C})$ *are Schur stable, where*

$$\mathcal{A} = \begin{bmatrix} A & FC_w \\ 0_{p \times n} & A_w \end{bmatrix}, \qquad \mathcal{C} = \begin{bmatrix} C & 0_{p \times q} \end{bmatrix}. \tag{4}$$

Assumption 6. *There exists synchronization between the clocks of the sensor, actuator and controller devices. Indeed, sensor and actuator are assumed to be located closed to the plant and governed by the same clock. But, as the controller is remotely located, in order to be synchronized with the local devices, a synchronization protocol for networks can be used [11].*

2.1. Packet dropouts and packet disorder

This section illustrates that both packet dropouts and packet disorder can be treated as time-varying delays. For instance, several consecutive packet dropouts lead to a monotonically increasing delay if the last received packet is processed at each *vacant* sampling (see Fig. 2), which is consistent with Assumption 2. Packet disorder can be detected by simply comparing the timestamps corresponding to the last received data packet with the stored one, before updating the local buffer: if the timestamp of the most recently received data packet is older than the timestamp of the stored one, we have a packet disorder. In this case, data packets containing older information are replaced by the newer ones, and hence discarded [5]. Thus, packet disorders can be treated as packet dropouts, and therefore as time-varying delays.

To better illustrate this, let us consider the example given in Fig. 3, where the data packets $p[1]$, $p[4]$ are lost, and $p[2]$, $p[3]$ are subject to packet disorder. Note from Fig. 3 that the received data packet $p[2]$ is older than the currently available $p[3]$ in the local receiver buffer. Therefore, $p[2]$ is discarded (and hence faced as a packet dropout). Hence, it can

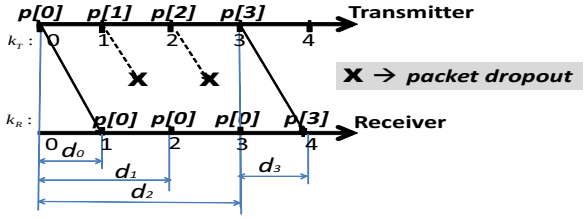

Figure 2: Illustration of a monotonically increasing time-varying delay $d_k = \{d_0, d_1, d_2, d_3\} = \{1, 2, 3, 1\}$ caused by packet dropouts ($p[1]$ and $p[2]$).

be deduced from Fig. 3 that such phenomena leads to time-varying delays d_k: $\{d_0, d_1, d_2, d_3, d_4, d_5, d_6\} = \{1, 2, 3, 1, 2, 3, 2\}$. Therefore, the time-varying network-induced delays d_k^{SC}, d_k^{CA} include not only transmission delays, but also packet dropouts and packet disorder phenomena. Let us denote N^{CA} and $\tilde{h}_2^{CA}$ the maximum possible number of consecutive packet dropouts and the worst-case transmission delay in the controller-to-actuator link, respectively (the same definitions hold for N^{SC} and $\tilde{h}_2^{SC}$ in the sensor-to-controller link). It is easy to see the following equivalences:

$$h_2^{CA} = N^{CA} + \tilde{h}_2^{CA}, \quad h_2^{SC} = N^{SC} + \tilde{h}_2^{SC} \tag{5}$$

where h_2^{CA}, h_2^{SC} are the upper bounds for the input and output delays given in Assumption 3.

2.2. Timestamping-based delay measurement

Let $k_T = 0, 1, 2, ...$ and $k_R = 0, 1, 2, ...$ the value of each local clock corresponding to the transmitter and receiver devices respectively, which are assumed to be synchronized (see Assumption 6). Using the same notation as Fig. 2 and Fig. 3, the timestamp $T_{k_T} = k_T$ is assigned at each transmitted data packet, denoted by $p[T_{k_T}]$. Hence, the total discrete-time delay caused by transmission delays, packet dropout and packet disorder can be measured at the receiver by simply computing the difference $k_R - T_{k_T}$, where T_{k_T} is here the timestamp extracted from the most recently received data packet, available in the local buffer.

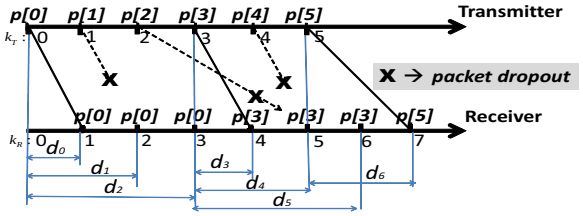

Figure 3: Illustration of the resulting time-varying delays $d_k = \{d_0, d_1, d_2, d_3, d_4, d_5, d_6\} = \{1, 2, 3, 1, 2, 3, 2\}$ caused by packet dropouts ($p[1]$ and $p[4]$) and packet disorder between data packets $p[2]$ and $p[3]$.

2.3. Preliminary results

Lemma 1. *Given any arbitrary discrete-time signal u_k, let $u_{d,k} = u_k - u_{k-1}$ and*

$$w_{d,k} = \frac{2}{\tau_{CA}} \left(u_{k-d_k^{CA}} - \frac{1}{2} \left(u_{k-h_1^{CA}} + u_{k-h_2^{CA}} \right) \right), \tag{6}$$

where $\tau_{CA} = h_2^{CA} - h_1^{CA}$. Then, the time-varying operator $\Delta_d : u_d \to w_d$ renders $w_{d,k} = \frac{1}{\tau_{CA}} \sum_{i=k-h_2^{CA}}^{k-h_1^{CA}-1} \phi(i) u_{d,i}$, where

$$\phi(i) = \begin{cases} 1 & \text{if } i < k - d_k^{CA} - 1, \\ -1 & \text{otherwise,} \end{cases} \tag{7}$$

and satisfies $||X \Delta_d X^{-1}||_\infty \leq 1$, for any invertible matrix X, where the symbol $||.||_\infty$ denotes the largest possible $\mathcal{L}_2$ induced norm of a general operator.

Proof: The proof is an adaptation of a similar result given in [43, Lemma 2] for continuous-time systems. Details are given in Appendix A. □

3. Proposed control strategy

Let us introduce the following event-triggered control strategy for the system (1):

$$u_k = \begin{cases} \tilde{u}_k & \text{if (9) is true} \\ u_{k-1} & \text{otherwise,} \end{cases} \tag{8}$$

where $\tilde{u}_k$ is defined later in (10), and the event-triggering condition (9) (given below) is used to decide whether the control action u_k must be sent to the actuator:

$$\left(\tilde{u}_k - u_{k-1}^T\right)^T \Omega_u \left(\tilde{u}_k - u_{k-1}^T\right) > \sigma_u \tilde{u}_k^T \Omega_u \tilde{u}_k, \tag{9}$$

being $\Omega_u \in \mathcal{R}^m$, and the positive scalar σ_u, some parameters to be designed. Given the controller parameters K, K_w to be later designed, let us define $\tilde{u}_k$ in (8) as

$$\tilde{u}_k = K_z \hat{z}_k + K_w \hat{\omega}_k, \tag{10}$$

where

$$K_z = 2K \left(A^{-h_1^{CA}} + A^{-h_2^{CA}}\right)^{-1}, \tag{11}$$

and $\hat{\omega}_k$, $\hat{z}_k$ are observed states, which respectively correspond to the disturbance component ω_k, and the following Arstein's state transformation z_k with delays h_1^{CA} and h_2^{CA}:

$$z_k = x_k + \Phi_k(h_1^{CA}) + \Phi_k(h_2^{CA}), \tag{12}$$

where

$$\Phi_k(h_i^{CA}) = \frac{1}{2} \sum_{i=0}^{h_i^{CA}-1} A^{-i-1} B u_{k-h_i^{CA}+i}. \qquad i = 1, 2. \tag{13}$$

The observed states $\hat{z}_k$, $\hat{\omega}_k$ are obtained from the gain-scheduled predictor-based ESO:

$$\hat{\tilde{z}}_{k+1} = \mathcal{A} \hat{\tilde{z}}_k + \tilde{\mathcal{B}} u_k + \mathcal{A}^{d_k^{SC}} \mathcal{L} e_k, \tag{14}$$

where $\mathcal{L}$ is the observer gain to be designed, and

$$\tilde{\mathcal{B}} = \begin{bmatrix} \tilde{B} \\ 0_{q \times m} \end{bmatrix}, \quad \tilde{B} = \frac{1}{2} \left(A^{-h_1^{CA}} + A^{-h_2^{CA}}\right) B, \tag{15}$$

being $\hat{\tilde{z}}_k = \begin{bmatrix} \hat{z}_k^T & \hat{\omega}_k^T \end{bmatrix}^T$, and e_k the observer error, defined as:

$$\begin{aligned} e_k = {} & \tilde{y}_{k-d_k^{SC}} - \mathcal{C} \mathcal{A}^{-d_k^{SC}} \hat{\tilde{z}}_k \\ & + C A^{-d_k^{SC}} \left(\Phi_k(h_1^{CA}) + \Phi_k(h_2^{CA}) + \Omega_k(d_k^{SC})\right), \end{aligned} \tag{16}$$

where

$$\Omega_k(d_k^{SC}) = \sum_{i=0}^{d_k^{SC}-1} A^{d_k^{SC}-i-1} B u_{k-d_k^{SC}+i-d_{k-d_k^{SC}+i}^{CA}}. \tag{17}$$

Analogously to (8), the delayed measured output $\tilde{y}_k$ in (16) transmitted by the sensor to the controller is defined by applying the following event-triggering protocol in the sensor-to-controller link:

$$\tilde{y}_k = \begin{cases} y_k & \text{if (19) is true} \\ \tilde{y}_{k-1} & \text{otherwise,} \end{cases} \tag{18}$$

where y_k is the output measurement given in (1), and the event-triggering condition in the sensor device is defined below:

$$\left(y_k - \tilde{y}_{k-1}^T\right)^T \Omega_y \left(y_k - \tilde{y}_{k-1}^T\right) > \sigma_y y_k^T \Omega_y y_k, \tag{19}$$

being $\Omega_y \in \mathcal{R}^p$, and the positive scalar σ_y, some parameters to be designed. Thus, the measurement data packets will be transmitted from the local sensor to the remote controller if the condition (19) is satisfied.

We emphasize that the control and observer gains K_w, K and $\mathcal{L}$ defined in (10), (11) and (14) respectively, together with the event-triggered parameters $\Omega_u, \sigma_u, \Omega_y, \sigma_y$ defined in (9) and (19), are designed not only to stabilize the closed-loop control system, but also to reduce the bandwidth usage as far as possible, while satisfying different performance criterions: maximum disturbance attenuation in the sense of H_∞ norm, steady-state rejection of mismatched disturbances with known dynamics, and robustness against time-varying delays.

Remark 1. *Note that, by setting $\sigma_u = 0$ and $\sigma_y = 0$ in (9) and (19) respectively, a time-triggered control is obtained with sampling period T_s. Therefore, a minimum sampling period equivalent to T_s is always guaranteed, preventing the occurrence of Zeno-behavior.*

Remark 2. *The event-triggered control scheme (8) without input delay compensation can be formulated by replacing K_z and $\hat{z}_k$ by K and $\hat{x}_k$ in (10), respectively:*

$$\tilde{u}_k = K\hat{x}_k + K_w\hat{\omega}_k, \tag{20}$$

where $\hat{x}_k$ is the observed plant state, obtained by means of the ESO:

$$\begin{aligned}\hat{\tilde{x}}_{k+1} &= \mathcal{A}\hat{\tilde{x}}_k + \mathcal{B}u_k + \mathcal{L}\left(\tilde{y}_{k-d_k^{SC}} - \mathcal{C}\hat{\tilde{x}}_k\right), \\ \mathcal{B} &= \begin{bmatrix} B^T & 0_{m\times q}\end{bmatrix}^T,\end{aligned} \tag{21}$$

where $\hat{\tilde{x}}_k^T = \begin{bmatrix}\hat{x}_k^T & \hat{\omega}_k^T\end{bmatrix}$. Note that (20) and (21) are respectively obtained from (8) and (14) by setting $h_1^{CA} = h_2^{CA} = h_1^{SC} = h_2^{SC} = 0$. Therefore, in the absence of time delays, the expressions (10), (14) and (20), (21) are equivalent. The above control scheme without delay compensation will be used to illustrate the benefits of using predictor-approaches in Section 6 (Example 2) and experimental results in Section 7. Some key aspects, such as the closed-loop performance and the achieved percentage ratio of transmitted packets by means of event-triggered protocols will be compared and discussed.

3.1. Delay-free interconnected state-space model

In this section, we show that the closed-loop control formed by the system (1) and the control law (8) can be described by an equivalent delay-free interconnected model (see Lemma 2 below). This result will be helpful to address later the stability analysis of the closed-loop control system.

Lemma 2. *The closed-loop system (1) with (8) can be modeled as the interconnected system formed by the delay-free model M_S and the feedback system Δ:*

$$\begin{aligned} M_S &: \begin{cases} \xi_{k+1} = \bar{A}_k\xi_k + \bar{G}_k\bar{w}_k + \bar{F}w_k, \\ \bar{y}_k = \bar{H}\xi_k + \bar{D}\bar{w}_k + \bar{J}w_k \end{cases}, \\ \Delta &: \begin{cases} \bar{w}_k = \bar{\Delta}_k\bar{y}_k, \end{cases} \end{aligned} \tag{22}$$

where $\bar{\Delta}_k$ is an unknown time-varying operator having block-diagonal structure: $\bar{\Delta}_k = diag\left(\Delta_d,\ \Delta_\eta,\ \Delta_\rho^*,\ \Delta_\nu\right)$ with $\Delta_d \in \mathcal{R}^m$, $\Delta_\eta \in \mathcal{R}^m$, $\Delta_\rho^* \in \mathcal{R}^p$, $\Delta_\nu \in \mathcal{R}^{n\times m}$, and satisfying $||T_1\bar{\Delta}T_2^{-1}||_\infty \leq 1$, where the scaling factors T_1 and T_2 are defined as:

$$\begin{aligned} T_1 &= diag\left(X,\ X_u,\ X_y,\ I_n\right), \\ T_2 &= diag\left(X,\ X_u,\ X_y,\ I_m\right), \\ X_u^T X_u &= \Omega_u, \qquad X_y^T X_y = \Omega_y \end{aligned} \tag{23}$$

and

$$\xi_k^T = \begin{bmatrix} z_k^T & u_{k-1}^T & \bar{e}_k^T \end{bmatrix}, \qquad \bar{e}_k = \bar{z}_k - \hat{\bar{z}}_k, \qquad \mathcal{K} = \begin{bmatrix} K_z & K_w \end{bmatrix} \tag{24}$$

$$\bar{A}_k = \begin{bmatrix} A + \tilde{B}K_z & 0 & -\tilde{B}\mathcal{K} \\ K_z & 0 & -\mathcal{K} \\ 0 & 0 & \mathcal{A} - \mathcal{A}^{d_k^{SC}} \mathcal{L}\mathcal{C} \mathcal{A}^{-d_k^{SC}} \end{bmatrix},$$

$$\bar{G}_k = \begin{bmatrix} G & \sqrt{\sigma_u}\tilde{\mathcal{B}} & 0 & 0 \\ 0 & 0 & 0 & 0 \\ \mathcal{G} & 0 & -\tau_{SC}\sqrt{\sigma_y}\mathcal{A}^{d_k^{SC}}\mathcal{L} & 0 \end{bmatrix}, \quad \bar{F} = \begin{bmatrix} F + \tilde{B}K_w \\ K_w \\ 0 \end{bmatrix},$$

$$\bar{H} = \begin{bmatrix} K_z & -I_m & -\mathcal{K} \\ K_z & 0 & -\mathcal{K} \\ C & C\Gamma_1 & 0 \\ K_z & -I_m & -\mathcal{K} \end{bmatrix}, \quad \bar{D} = \begin{bmatrix} 0 & \sqrt{\sigma_u} I_m & 0 & 0 \\ 0 & 0 & 0 & 0 \\ 0 & 0 & 0 & \mu C \\ 0 & \sqrt{\sigma_u} I_m & 0 & 0 \end{bmatrix},$$

$$\bar{J}^T = \begin{bmatrix} K_w^T & K_w^T & 0 & K_w^T \end{bmatrix},$$

$$\Gamma_1 = \left(\sum_{j=0}^{h_1^{CA}-1} A^{-j-1} + \sum_{j=0}^{h_2^{CA}-1} A^{-j-1} \right) \frac{B}{2},$$

$$\mu = \left\| \sum_{r=1}^{2} \sum_{j=0}^{h_r^{CA}-1} \sum_{f=1}^{h_r^{CA}-j-1} A^{-j-1} \frac{B}{2} z^{-f} \right\|_\infty,$$

where $\tilde{B}$ *and* K_z *are defined in* (15) *and* (11) *respectively. The symbol* z *given in the above defined parameter* μ *stands for the discrete-time operator.*

Proof: See Appendix A. □

The corollary given below (Corollary 1) shows that the closed-loop poles of the control system, which are equivalent to the eigenvalues of $\bar{A}_k$ in (24), are independent of the instant values of time delays d_k^{SC} and d_k^{CA}, and equivalent to the eigenvalues of $(A + BK)$ and $(\mathcal{A} - \mathcal{L}\mathcal{C})$.

Corollary 1. *The time-varying matrix* $\bar{A}_k$ *defined in* (24) *has* m *eigenvalues equal to 0, and the rest of them are the eigenvalues of matrices* $(A + BK)$ *and* $(\mathcal{A} - \mathcal{L}\mathcal{C})$, $\forall k \geq 0$.

Proof: Noting the block-triangular structure of $\bar{A}_k$:

$$\bar{A}_k = \left[\begin{array}{cc|c} A+\tilde{B}K_z & 0 & -\tilde{B}\tilde{K} \\ K_z & 0_m & -\tilde{K} \\ \hline 0 & 0 & \mathcal{A}-\mathcal{A}^{d_k^{SC}}\mathcal{L}\mathcal{C}\mathcal{A}^{-d_k^{SC}} \end{array}\right],$$

it can easily be deduced that its eigenvalues are the eigenvalues of the matrices $\bar{A}_1$ and $\bar{A}_{2,k}$, where:

$$\bar{A}_1 = \begin{bmatrix} A+\tilde{B}K_z & 0 \\ K_z & 0_m \end{bmatrix}, \qquad \bar{A}_{2,k} = \mathcal{A}-\mathcal{A}^{d_k^{SC}}\mathcal{L}\mathcal{C}\mathcal{A}^{-d_k^{SC}}.$$

Note that the matrix $\bar{A}_1$ has m eigenvalues equal to 0, and the rest of them are the eigenvalues of $(A+\tilde{B}K_z)$. Finally, the proof can be completed by taking into account that:

- (i) The eigenvalues of $(A+BK)$ are the same as $\Xi_2(A+BK)\Xi_2^{-1}$ for any regular matrix Ξ_2. Therefore, by choosing

  $$\Xi_2 = 0.5\left(A^{-h_1^{CA}}+A^{-h_2^{CA}}\right),$$

  we have that $\Xi_2 A \Xi_2^{-1} = A$. Also, taking into account from (15) and (11) that $\tilde{B} = \Xi_2 B$ and $K_z = K\Xi_2^{-1}$ respectively, we deduce that $(A+\tilde{B}K_z)$ has the same eigenvalues as $(A+BK)$.

- (ii) The eigenvalues of $(\mathcal{A}-\mathcal{L}\mathcal{C})$ are the same as $\Xi_1(\mathcal{A}-\mathcal{L}\mathcal{C})\Xi_1^{-1}$ for any regular matrix Ξ_1. Therefore, by choosing $\Xi_1 = \mathcal{A}^{d_k^{SC}}$, we deduce that $\bar{A}_{2,k}$ has the same eigenvalues as $(\mathcal{A}-\mathcal{L}\mathcal{C})$, for any d_k^{SC}.

□

Remark 3. *Note that the current and past measured delays d_k^{SC}, d_k^{CA} comprising transmission delays, packet loss and packet disorder (as explained in Section 2.1 and Section 2.2) are used to update the control scheme during control execution by means of the gain-scheduling law given in* (14), (16) *and* (17). *Corollary 1 reveals that closed-loop system behavior approaches to the nominal closed-loop performance given by the eigenvalues of $(A+BK)$ and $(\mathcal{A}-\mathcal{L}\mathcal{C})$ for sufficiently slow time-varying delays, no matter how long they are. Hence, it can be seen that this key feature is achieved thanks to the proposed gain-scheduled observer, in combination with the predictor-based control scheme.*

4. Stability analysis

The following theorem enables to prove the stability with decay-rate $0 < \beta \leq 1$ of the closed-loop system (1) with the control law (8) and the predictor-observer scheme (14), for any arbitrarily fast-time varying delays d_k^{SC}, d_k^{CA}.

Theorem 1. *Given $\mathcal{K}$, $\mathcal{L}$, and scalars σ_u, σ_y, h_1^{SC}, h_2^{SC}, h_1^{CA}, $h_2^{CA} > 0$, the closed-loop system* (1) *with the control law* (8) *and the predictor-observer scheme* (14) *is robustly asymptotically stable with decay rate β if there exist symmetric matrices $P \in \mathcal{R}^{2n+m+q} > 0$, $\tilde{S} \in \mathcal{R}^m > 0$, $\tilde{\Omega}_u \in \mathcal{R}^m > 0$, $\tilde{\Omega}_y \in \mathcal{R}^p > 0$ and a scalar $\rho > 0$, such that the following LMIs are satisfied, $\forall i = 1, \cdots, h_2^{SC} - h_1^{SC} + 1$:*

$$\hat{\Gamma}_i < 0, \tag{25}$$

where

$$\hat{\Gamma}_i = \begin{bmatrix} -\beta^2 P & 0 & 0 & P\hat{\bar{A}}_i^T & P\bar{H}^T & P\bar{C}_s^T \\ (*) & -\mathcal{W}_1 & 0 & \mathcal{W}_1\hat{\bar{G}}_i^T & \mathcal{W}_1\bar{D}^T & \mathcal{W}_1\bar{D}_s^T \\ (*) & (*) & -\rho I_q & \bar{F}^T & \bar{J}^T & 0 \\ (*) & (*) & (*) & -P & 0 & 0 \\ (*) & (*) & (*) & (*) & -\mathcal{W}_2 & 0 \\ (*) & (*) & (*) & (*) & (*) & -I_{p_s} \end{bmatrix}, \tag{26}$$

and

$$\hat{\bar{A}}_i = \begin{bmatrix} A + \tilde{B}K_z & 0 & -\tilde{B}\mathcal{K} \\ K_z & 0 & -\mathcal{K} \\ 0 & 0 & \mathcal{A} - \mathcal{A}^{d_i}\mathcal{L}\mathcal{C}\mathcal{A}^{-d_i} \end{bmatrix}, \tag{27}$$

$$\hat{\bar{G}}_i = \begin{bmatrix} G & \sqrt{\sigma_u}\tilde{B} & 0 & 0 \\ 0 & 0 & 0 & 0 \\ \mathcal{G} & 0 & -\tau_{SC}\sqrt{\sigma_y}\mathcal{A}^{d_i}\mathcal{L} & 0 \end{bmatrix},$$

$$\mathcal{W}_1 = diag\left(\tilde{S},\ \tilde{\Omega}_u,\ \tilde{\Omega}_y,\ I_m\right),$$

$$\mathcal{W}_2 = diag\left(\tilde{S},\ \tilde{\Omega}_u,\ \tilde{\Omega}_y,\ I_n\right),$$

$$\bar{C}_s = \begin{bmatrix} C_s & C_s\Gamma_1 & 0 \end{bmatrix}, \quad \bar{D}_s = \begin{bmatrix} 0 & 0 & 0 & \mu C_s \end{bmatrix},$$

$$\rho = \gamma^2, \qquad \tau_{SC} = h_2^{SC} - h_1^{SC}, \qquad \tau_{CA} = h_2^{CA} - h_1^{CA}.$$

where $d_i = h_1^{SC} + i - 1$, and $\bar{F}, \bar{H}, \bar{D}, \bar{J}$, Γ_1 and μ are defined in (24)*. In addition, the event-triggered parameters Ω_u, Ω_y are obtained as $\Omega_u = \tilde{\Omega}_u^{-1}$, $\Omega_y = \tilde{\Omega}_y^{-1}$.*

Proof: See Appendix B. □

Remark 4. *The H_∞ disturbance rejection performance $\gamma = \sqrt{\rho}$ can be obtained from Theorem 1 by solving the following convex optimization problem:*

$$min\ \rho\ s.t\ \ LMIs\ (25) \tag{28}$$

5. Control synthesis

Note that the matrix inequalities (25) are not linear if the control and observer gains K and $\mathcal{L}$ are defined as LMI decision variables. Therefore, the problem of control synthesis by means of Theorem (1) or (28) renders non convex. In this section, we propose a Cone Complementarity Linearization (CCL) algorithm to find the values of K and $\mathcal{L}$ that enhance as long as possible some of the following closed-loop performance indices: maximum allowable delays τ_{SC}, τ_{CA}, bandwidth usage through the event-triggered parameters σ_u, σ_y, decay rate performance β, and the H_∞ disturbance rejection γ corresponding to the transfer function between the disturbance input w_k and the controlled output $y_{s,k}$.

Note that, by denoting $Q = P^{-1}$ and $\mathcal{X}_y = \Omega_y^{-1}$ in (75), and pre-and post multiplying by $diag\left(I, \tilde{\mathcal{W}}_1, I, I, I, I\right)$ (where $\tilde{\mathcal{W}}_1$ is defined below), we obtain:

$$\hat{\Gamma}_i^* = \begin{bmatrix} -\beta^2 Q & 0 & 0 & \hat{\bar{A}}_i^T & \bar{H}^T & \bar{C}_s^T \\ (*) & -\tilde{\mathcal{X}}_1 & 0 & \tilde{\mathcal{W}}_1 \hat{\bar{G}}_i^T & \tilde{\mathcal{W}}_1 \bar{D}^T & \tilde{\mathcal{W}}_1 \bar{D}_s^T \\ (*) & (*) & -\gamma^2 I_q & \bar{F}^T & \bar{J}^T & 0 \\ (*) & (*) & (*) & -P & 0 & 0 \\ (*) & (*) & (*) & (*) & -\mathcal{W}_2 & 0 \\ (*) & (*) & (*) & (*) & (*) & -I_{p_s} \end{bmatrix},$$

$$\tilde{\mathcal{W}}_1 = diag\left(S,\ \Omega_u,\ I_p,\ I\right), \tag{29}$$

$$\tilde{\mathcal{X}}_1 = diag\left(S,\ \Omega_u,\ \mathcal{X}_y,\ I\right)$$

Also, let us introduce the LMI conditions to relax the equality constraints $PQ = I$ and $\Omega_y \mathcal{X}_y = I$ for the CCL algorithm:

$$\begin{bmatrix} P & I \\ I & Q \end{bmatrix} \geq 0, \quad \begin{bmatrix} \Omega_y & I \\ I & \mathcal{X}_y \end{bmatrix} \geq 0, \tag{30}$$

together with the objective function to minimize:

$$\min(\text{trace}(PQ + QP + \Omega_y \mathcal{X}_y + \mathcal{X}_y \Omega_y)). \tag{31}$$

5.1. CCL algorithm description

Let σ_u, σ_y, β and γ the performance indices to be improved for control design, and let δ_σ^u, δ_σ^y, δ_β and δ_γ their corresponding incremental values for each iteration. For instance, if one were only interested in finding a control which only maximizes σ_y as much as possible, the increment δ_σ^y should be defined strictly positive, and the rest of incremental values should be set at zero. The algorithm is described below:

- Step (i): Design K and $\mathcal{L}$ such that $A+BK$ and $\mathcal{A}-\mathcal{L}\mathcal{C}$ are Schur-stable, and K_w to achieve a null steady-state error of the external disturbance w_k.

- Step (ii): Solve the convex optimization problem (28) taking a sufficiently positive small values for $\sigma_u = \sigma_u^0$, $\sigma_y = \sigma_y^0$, and $\beta = \beta^0$ to find a feasible solution. Set $q = 0$, $P_0 = P, Q_0 = P^{-1}, \Omega_{y,0} = \Omega_y, \mathcal{X}_{y,0} = \Omega_y^{-1}$ and $\gamma^0 = \sqrt{\rho}$.

- Step (iii): Solve the convex optimization problem min(trace($P_qQ + Q_qP + \Omega_{y,q}\mathcal{X}_y + \mathcal{X}_{y,q}\Omega_y$)) subjet to the LMI's (30) and $\hat{\Gamma}_i^* < 0$, $i = 1, ..., h_2^{SC} - h_1^{SC} + 1$, where $\hat{\Gamma}_i^*$ is defined in (29), considering $\sigma_u = \sigma_u^q + \delta_\sigma^u$, $\sigma_y = \sigma_y^q + \delta_\sigma^y$, $\beta = \beta^q - \delta_\beta$ and $\gamma = \gamma^q + \delta_\gamma$, where $\hat{\Gamma}_i^*$ is defined in (29), and $P, Q, S, \Omega_u, \Omega_y > 0, K, K_w, \mathcal{L}$ are decision variables.

- Step (iv): If a feasible solution is found, go to step (v). Otherwise, set $\delta_\sigma^u = \delta_\sigma^u/h$, $\delta_\sigma^y = \delta_\sigma^y/h$, $\delta_\beta = \delta_\beta/h$ and $\delta_\gamma = \delta_\gamma/h$, for some $h > 1$, until a feasible solution is found in Step (iii).

- Step (v): Check if (25) hold with the obtained values in Step (iv) taking $P = m_1P^* + (1-m_1)(Q^*)^{-1}$ and $\Omega_y = m_2\Omega_y^* + (1-m_2)\left(\mathcal{X}_y^*\right)^{-1}$, for some $0 \leq m_i \leq 1$, $i = 1, 2$, where P^*, Q^*, Ω_y^* and $\mathcal{X}_y^*$ are the feasible solutions obtained in Step (iii). If the inequalities (25) are true, go to Step (vi). Otherwise, set $\delta_\sigma^u = \delta_\sigma^u/h$, $\delta_\sigma^y = \delta_\sigma^y/h$, $\delta_\beta = \delta_\beta/h$ and $\delta_\gamma = \delta_\gamma/h$, for some $h > 1$, and execute Steps (iii),(iv) and (v) until a feasible solution is found.

- Step (vi): If the maximum number of iterations is still not reached, set $q = q+1$, $P_q = P_{q-1}$, $Q_q = P_{q-1}^{-1}$, $\sigma_u^q = \sigma_u^{q-1}$, $\sigma_y^q = \sigma_y^{q-1}$, $\epsilon_\beta^q = \epsilon_\beta^{q-1}$, $\epsilon_\gamma^q = \epsilon_\gamma^{q-1}$ and go to Step (iii). Otherwise, stop and exit.

6. Simulation results

Two examples are provided in this section. The first example shows the effectiveness of the proposed control synthesis algorithm in an open-loop unstable plant brought from the literature, but including mismatched disturbances. The second example illustrates the advantages of predictor-based control approaches in terms of closed-loop performance and bandwidth usage, considering the same plant model as the experimental setup.

6.1. Example 1

Consider the open-loop unstable plant studied in [24], where rejection of mismatched disturbances has been carried out by the proposed gain-scheduled ESO (which is an improvement of our work compared to the one in [24]). Let $T_s = 0.1s$ be the sampling period. The discrete-time system model (1) renders:

$$A = \begin{bmatrix} 1.0101 & 0.0600 \\ 0 & 0.9900 \end{bmatrix}, \quad B = \begin{bmatrix} 0.1035 \\ 0.0995 \end{bmatrix}, \quad C = \begin{bmatrix} 1 & 1 \end{bmatrix}. \tag{32}$$

For simulation purposes, we introduce the following disturbance input w_k, where the component ω_k with known dynamics is assumed to be on the form:

$$\omega_k = \begin{cases} 0 & \text{if } t < 9s \;||\; t > 27s \\ -0.2 & \text{otherwise.} \end{cases} \tag{33}$$

and the unknown component $w_{u,k}$ is a randomly generated signal with maximum amplitude 0.05.

Let $F = B$, $C_s = [0,\ 1]$. Also, from (33), we can deduce that ω_k can be modeled using (3) with $A_w = 1$, $C_w = 1$. Now, let us consider the proposed event-triggered control scheme (8)-(19) by choosing K and $\mathcal{L}$ (see below), such that $A + BK$ and $\mathcal{A} - \mathcal{L}\mathcal{C}$ are Schur-stable matrices:

$$\begin{aligned} &K = \begin{bmatrix} -0.2951 & -0.4439 \end{bmatrix}, \\ &\mathcal{L} = \begin{bmatrix} 83.8702 & -81.3701 & 21.9998 \end{bmatrix}^T, \quad K_w = -1.1511, \\ &\sigma_u = 3 \cdot 10^{-4}, \quad \sigma_y = 3 \cdot 10^{-5}, \quad \Omega_u = \Omega_y = 1. \end{aligned} \tag{34}$$

where K_w has been set to achieve a steady-state rejection of any unknown input disturbance w_k of step form. By means of Theorem 1, we prove that

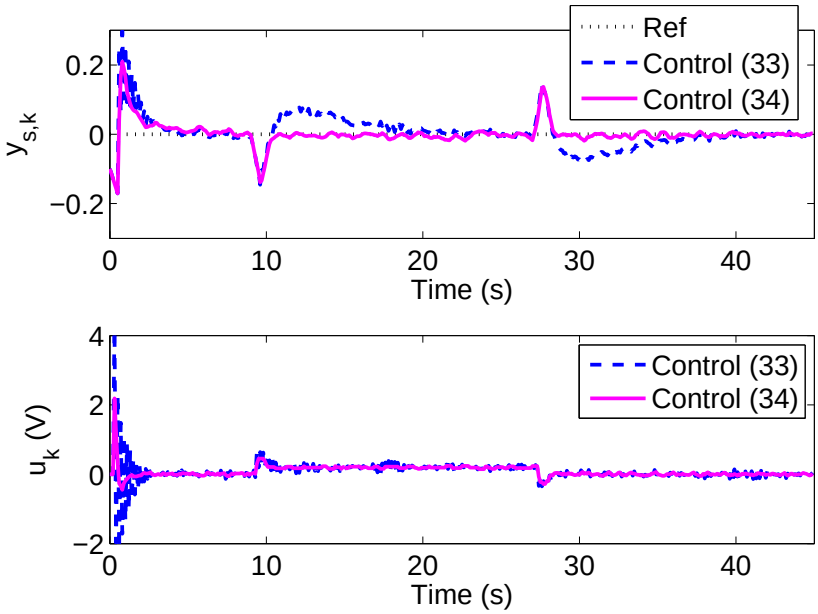

Figure 4: (Example 1) Comparative results between the control settings (34) and (35) for $d_k^{SC} = 2$, $d_k^{CA} = 2$ using the proposed control scheme (8)-(19).

the closed-loop system formed with K, K_w and $\mathcal{L}$ given in (34) is stable up to $\sigma_u = 3 \cdot 10^{-4}$, $\sigma_y = 3 \cdot 10^{-5}$ with H_∞ performance $\gamma = 38.6275$, by setting $\beta = 0.996$ and $d_k^{SC} = d_k^{CA} = 2$.

With the objective of reducing the bandwidth usage and improve the H_∞ performance at the same time, we design by the proposed algorithm in Section 5.1 a new control and observer gains. Since $A + BK$ and $\mathcal{A} - \mathcal{L}\mathcal{C}$ are Schur-stable matrices, Corollary 1 ensures the closed-loop stability for any time-constant delays. Therefore, we have used K, K_w and $\mathcal{L}$ in (34) as starting values for step (i) in the given algorithm. As a result, we obtain the

Control setting	$CA(\%)$	$SC(\%)$
See (34)	**99.34**	**98.66**
See (35)	**64.44**	**92.00**

Table 1: (Example 1) Comparison of the percentage of transmitted packets in both channels (columns $SC(\%)$ and $CA(\%)$) for $d_k^{SC} = 2$, $d_k^{CA} = 2$ between the control settings (34) and (35) using the proposed control scheme (8)-(19).

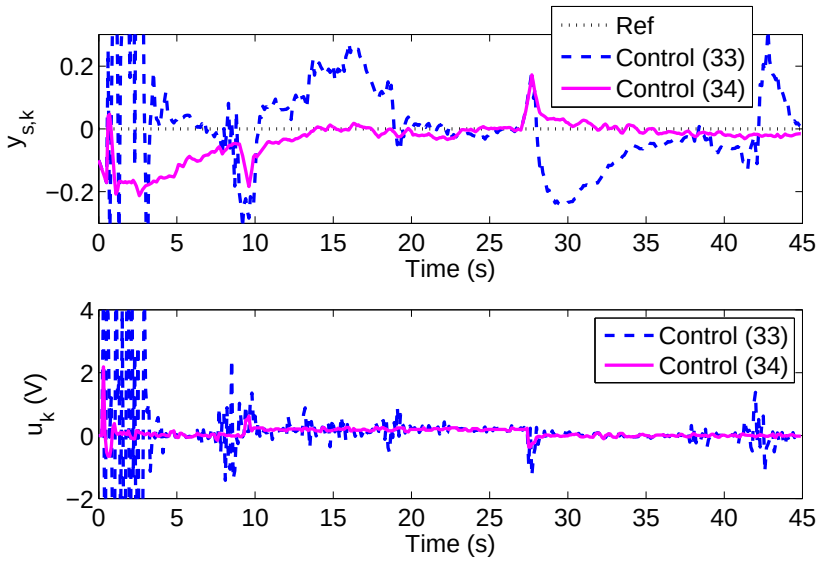

Figure 5: (Example 1) Comparative results between the control settings (34) and (35) for $1 \leq d_k^{SC} \leq 3$, $d_k^{CA} = 2$ using the proposed control scheme (8)-(19).

following control and observer gains:

$$\begin{aligned} K &= \begin{bmatrix} -0.2771 & -0.4728 \end{bmatrix}, \\ \mathcal{L} &= \begin{bmatrix} 84.8702 & -83.3701 & 19.9998 \end{bmatrix}^T, \quad K_w = -1.1529, \\ \sigma_u &= 0.9 \cdot 10^{-2}, \quad \sigma_y = 2.4 \cdot 10^{-3}, \quad \Omega_u = \Omega_y = 1, \end{aligned} \tag{35}$$

where better H_∞ performance $\gamma = 11.59$ has been obtained, in comparison to the original design given in (34). In this case, we have also set $\beta = 0.996$, and $d_k^{SC} = d_k^{CA} = 2$.

Control setting	$CA(\%)$	$SC(\%)$
See (34)	**97.81**	**99.11**
See (35)	**63.34**	**87.52**

Table 2: (Example 1) Comparison of the percentage of transmitted packets in both channels (columns $SC(\%)$ and $CA(\%)$) for $1 \leq d_k^{SC} \leq 3$, $d_k^{CA} = 2$ between the control settings (34) and (35) using the proposed control scheme (8)-(19).

Comparative simulation results are depicted in Table 1 and Fig. 4 assuming $d_k^{SC} = d_k^{CA} = 2$. It can be appreciated that the dynamic performance obtained by the designed control setting (35) (magenta solid-line) is better than (34) (blue dashed-line), which confirms the effectiveness of the control synthesis algorithm. Note also that the disturbance input w_k defined in (33) is effectively steady-state rejected in the controlled output $y_{s,k}$, as expected from the proposed ESO scheme.

Next, let $1 \leq d_k^{SC} \leq 3$, where comparative results are given in Fig. 5 and Table 2. Here we illustrate that the designed control scheme (35) (magenta solid-line) clearly outperforms the original design (34) (blue dashed-line) even in case of time-varying delays. For a fair comparison, the same time-varying patterns for delays and unknown disturbance $\omega_{u,k}$ have been used in both simulations.

Note also that a reduction of the transmitted data packets has been achieved in both cases. The ratio between transmitted data packets and total number of transmitted ones along the control execution is compared in Table 1 and Table 2 (see bold style) for time-constant and time-varying delay cases, respectively.

6.2. Example 2

Consider the NCS, where the plant model is described by (1), which is a discrete-time approximate model of the experimental platform used afterwards with sampling period $T_s = 0.01s$. The system matrices are:

$$A = \begin{bmatrix} 1 & 0.01 \\ 0 & 1 \end{bmatrix}, \; B = F = \begin{bmatrix} 0 \\ 0.001 \end{bmatrix}, \qquad (36)$$
$$C = C_s = \begin{bmatrix} 1 & 0 \end{bmatrix}.$$

Consider the following control and observer gains K and $\mathcal{L}$, already used in [14], to stabilize the system:

$$K = -\begin{bmatrix} 50 & 45 \end{bmatrix}, \quad \mathcal{L}^T = \begin{bmatrix} 0.57 & 3.62 & 60 \end{bmatrix}, \quad K_w = -1.9540, \qquad (37)$$

where K_w has been set to achieve a steady-state rejection of any unknown input disturbance w_k of step form.

For simulation purposes, we introduce a disturbance input signal $w_k = \omega_k$, where ω_k is defined as:

$$\omega_k = \begin{cases} 0 & \text{if } t < 30s \\ -2.5 & \text{otherwise,} \end{cases} \qquad (38)$$

Control	$SC(\%)$	$CA(\%)$
Delay-free case	**17.45%**	**22.55%**
Control without delay compensation	**89.43%**	**72.53%**
Proposed control scheme	**17.73%**	**34.30%**

Table 3: (Example 2) Comparison of the percentage of transmitted packets in both channels (columns $SC(\%)$ and $CA(\%)$) using different control schemes for $1 \leq d_k^{SC} \leq 17$, $1 \leq d_k^{CA} \leq 17$. The event-triggered parameters are $\sigma_u = 1 \cdot 10^{-2}$, $\Omega_u = 1$ and $\sigma_y = 1 \cdot 10^{-5}$, $\Omega_y = 1$.

Fig. 6 gives comparative results between the proposed control law (8)-(19) with respect to the control scheme without delay compensation (see Remark 2) using the control parameters given in (37). It can be appreciated that the achieved response (dash-dotted magenta line) appears to be very similar to the delay-free case (blue solid-line) using the proposed control scheme. Time-varying delay intervals have been chosen to be $1 \leq d_k^{SC} \leq 17$, $1 \leq d_k^{CA} \leq 17$ since such delay intervals lead the closed-loop system to the verge of instability (dashed green line) when no delay compensation is implemented. The event-triggered parameters have been set in all cases as $\sigma_u = 1 \cdot 10^{-2}$, $\Omega_u = 1$ and $\sigma_y = 1 \cdot 10^{-5}$, $\Omega_y = 1$. Note from Table 3 that the percentage of transmitted data packets in both channels is similar to the delay-free case using the proposed control, meanwhile such percentages are sensibly greater without delay compensation, even using the same threshold parameters. This fact can be explained because the convergence is faster and there are less oscillations using the proposed control scheme. Therefore, the average number of times that conditions (9), (19) are true is reduced, leading to less number of transmitted packets. For a fair comparison, the same time-varying delay patterns have been used in both simulations.

Fig. 7 gives comparative results using the proposed control law (8)-(19) with control parameters (37) under different event-triggered parameters. It can be seen that the closed-loop performance is hardly degraded for greater values of σ_u and σ_y, but an important reduction of transmitted data packets has been achieved in both channels (see Table 4). Note that by setting $\sigma_u = 0.1$ and $\sigma_y = 10^{-4}$ (see third row in Table 4), the percentage of transmitted data packets (13.15% and 22.31%) is less than the delay-free case (see first row in Table 3) (17.45% and 22.55%), while exhibiting a similar response (settling time around $5s$ and no overshoot) in both cases.

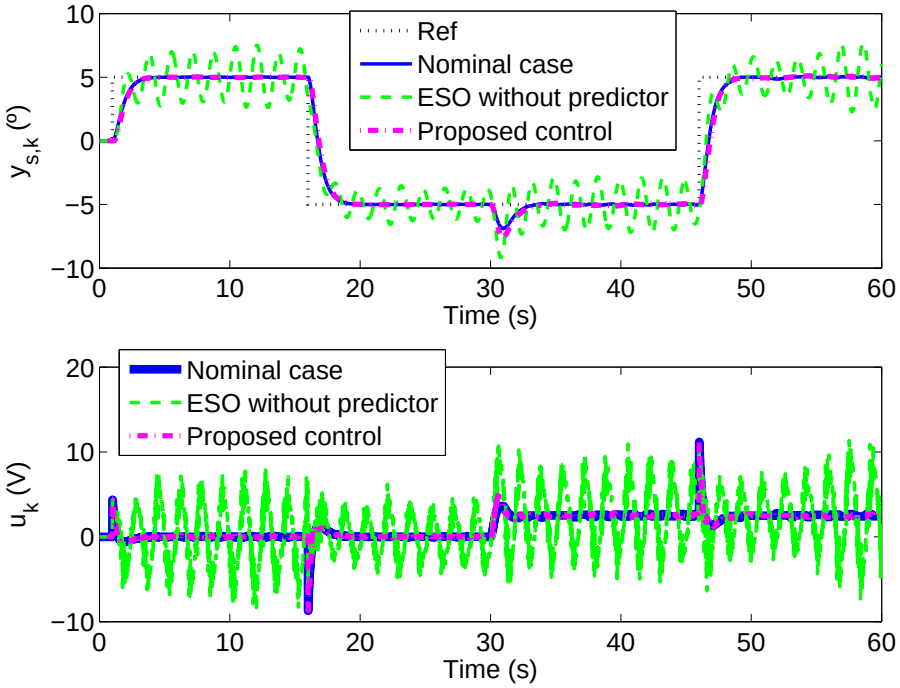

Figure 6: (Example 2) Comparison of the output system (upper part) and the control action (lower part) for $1 \leq d_k^{SC} \leq 17$, $1 \leq d_k^{CA} \leq 17$ using the proposed control scheme (8)-(19) with respect to the nominal delay-free case and the same control scheme without delay compensation. The event-triggered parameters are $\sigma_u = 1 \cdot 10^{-2}$, $\Omega_u = 1$ and $\sigma_y = 1 \cdot 10^{-5}$, $\Omega_y = 1$.

σ_u	σ_y	$SC(\%)$	$CA(\%)$
0.001	10^{-6}	**23.31%**	**42.58%**
0.01	10^{-5}	**17.60%**	**32.98%**
0.1	10^{-4}	**13.15%**	**22.31%**

Table 4: (Example 2) Comparison of the percentage of transmitted packets in both channels using the proposed control scheme and different event-triggered parameters σ_u, σ_y taking $\Omega_u = 1, \Omega_y = 1$ (columns $SC(\%)$ and $CA(\%)$). Time-varying delays have been chosen to be $1 \leq d_k^{SC} \leq 17$, $1 \leq d_k^{CA} \leq 17$

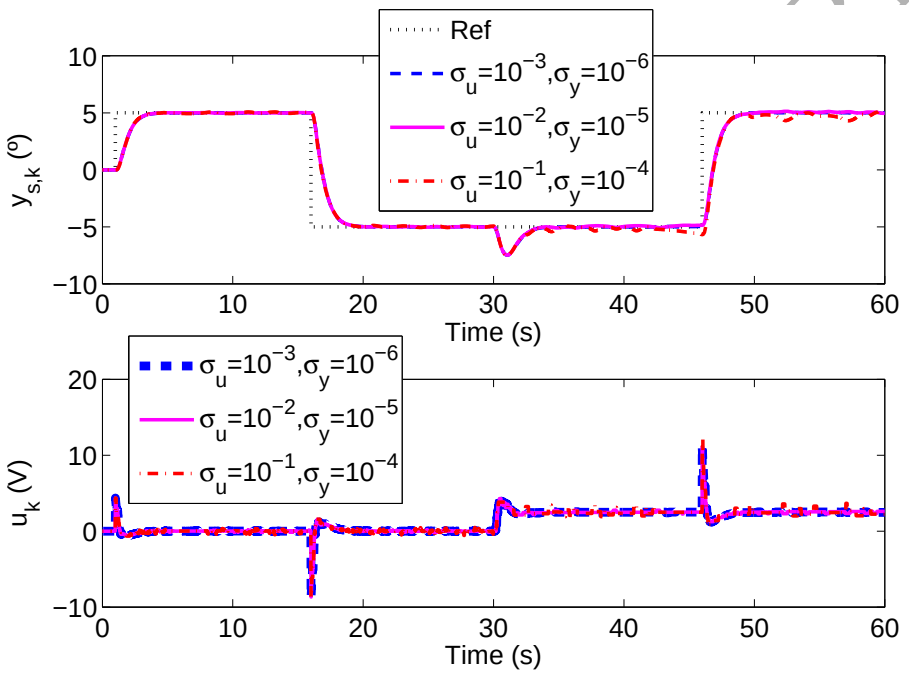

Figure 7: (Example 2) Comparison of the output system (upper part) and the control action (lower part) for $1 \leq d_k^{SC} \leq 17$, $1 \leq d_k^{CA} \leq 17$ using the proposed control scheme (8)-(19) using different event-triggered parameters σ_u, σ_y taking $\Omega_u = 1, \Omega_y = 1$).

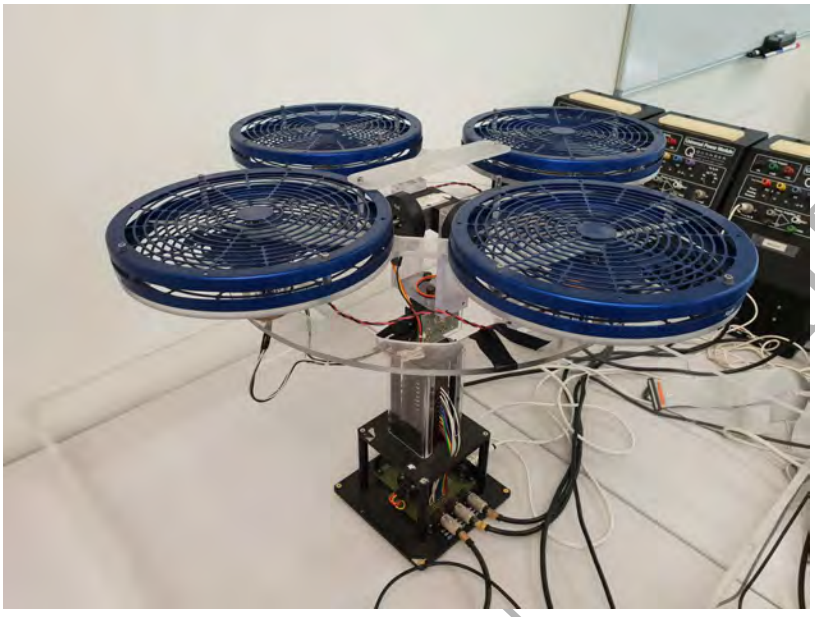

Figure 8: 3-DOF Hover of Quanser (experimental platform)

7. Experimental results

The proposed control law has been implemented in the 3DOF Hover of Quanser shown in Fig. 8. This test-bed consists of a quadrotor installed in a pivot joint, which enables it to spin in roll, pitch and yaw angles without translational movement. The angles are measured by optical encoders with an accuracy of 0.04°. The four motors of the system can be set between $-10V$ and $+10V$. Moreover, the motors present a dead zone between $\pm 0.5V$. The implemented control strategy has been executed in a PC with a real-time Linux OS distribution, which enables to run the full algorithm with a sampling time of $0.01s$. The computer is connected to the Quanser hardware by means of a data acquisition board with a resolution of $16bit$.

The experiment has been performed considering only the roll angle, which is denoted as $\theta(t)$. If the yaw and pitch angles are zero, the dynamics of $\theta(t)$ can be approximated by the following model [35]:

$$\ddot{\theta}(t) = K_s u(t) + w(t), \quad K_s = 0.1, \tag{39}$$

where $u(t)$ is the input voltage of the motors used to control the roll axis,

$K_s = 0.1$ is a constant representing the inertia moment, and $w(t)$ represents a load disturbance.

The discrete-time system model with sampling period $T_s = 0.01s$ is the same as Example 2, being (36) the system matrices. Moreover, the control and observer gains are given in (37).

Two comparative experiments have been carried out in order to illustrate the effectiveness of the proposed strategy: (i) a comparison among the ideal strategy (without delays), the control without delay compensation (see Remark 2) in the presence of time-varying delays, and the proposed control strategy in the presence of the same time-varying delays as the previous case, and (ii): a comparison using different values of σ_y and σ_u with the proposed control strategy, in order to illustrate the trade-off between performance and bandwidth usage.

For a fair comparison, both experiments have been carried out using the same time-varying delays, where $1 \leq d_k^O \leq 11$ and $1 \leq d_k^I \leq 10$. Such delay intervals have been selected in order to lead the system to the verge of instability in case of having no delay compensation, as discussed in Remark 2 (see case 1b in Fig. 9). The set-point changes between $-5°$ and $+5°$ (see black dotted-line in the upper side of Fig. 9). With the objective to illustrate the effectiveness of the ESO, the following load disturbance $w(t)$ has been introduced by software:

$$\omega_k = \begin{cases} 0\ V & \text{if } t < 30s \\ -2.5\ V & \text{otherwise.} \end{cases} \tag{40}$$

The closed-loop responses of the first and second experiments are depicted in Fig. 9 and Fig. 10, respectively. Table 5 shows the percentage of transmitted packets for the different experiments carried out in the second experiment. In light of the given results, a drastic bandwidth reduction can be appreciated, with a slight degradation of the system performance. It can also be appreciated the presence of some peaks in the interval $30s - 40s$ due to the load disturbance $w(t)$ given in (40), but after these peaks, the roll angle converges to the reference value (see Fig. 9). This fact reveals that the load disturbance $w(t)$ is effectively steady-state rejected in the controlled output (roll angle).

The results obtained in this section confirm the trends observed in the simulation example, and hence, the proposed control solution is experimentally validated.

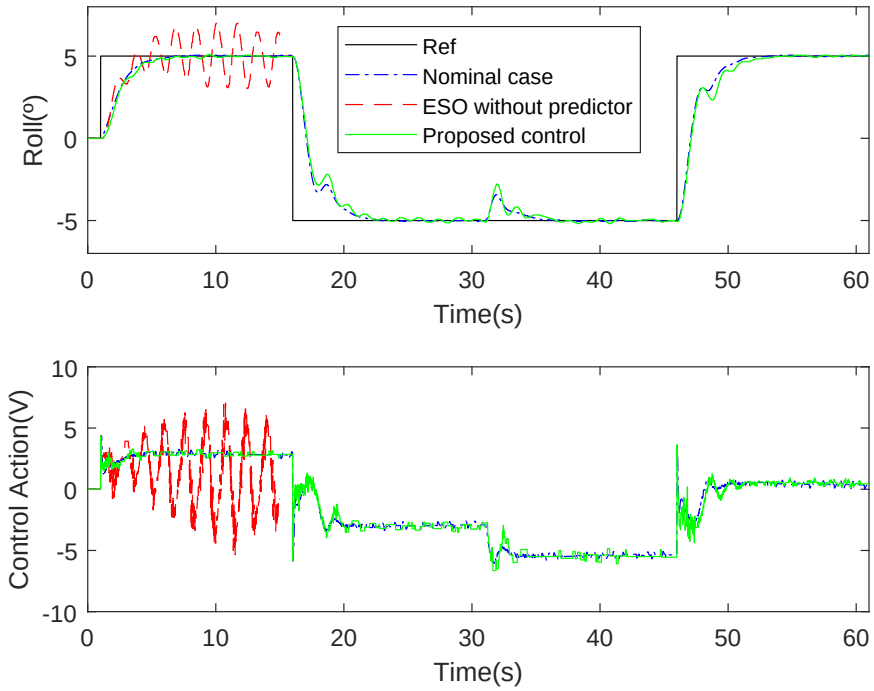

Figure 9: Experiment 1: Comparative among different control strategies. Ideal scheme (without delays), control with delays but not considering them for the design and Proposed scheme with delays ($\sigma_y = 1e-5$, $\sigma_u = 0.01$)

However, notice that delay intervals have been chosen both in the experimental setup and Example 2 to lead the closed-loop system without delay compensation to the limit of stability, with the objective of better highlighting the benefits of using predictor approaches. As could be expected, the maximum allowable delay intervals are smaller in the experimental setup than the obtained by simulation in Example 2. This fact explains why better reductions of transmitted packets are obtained in the experiments than simulation (Table 5 vs Table 4).

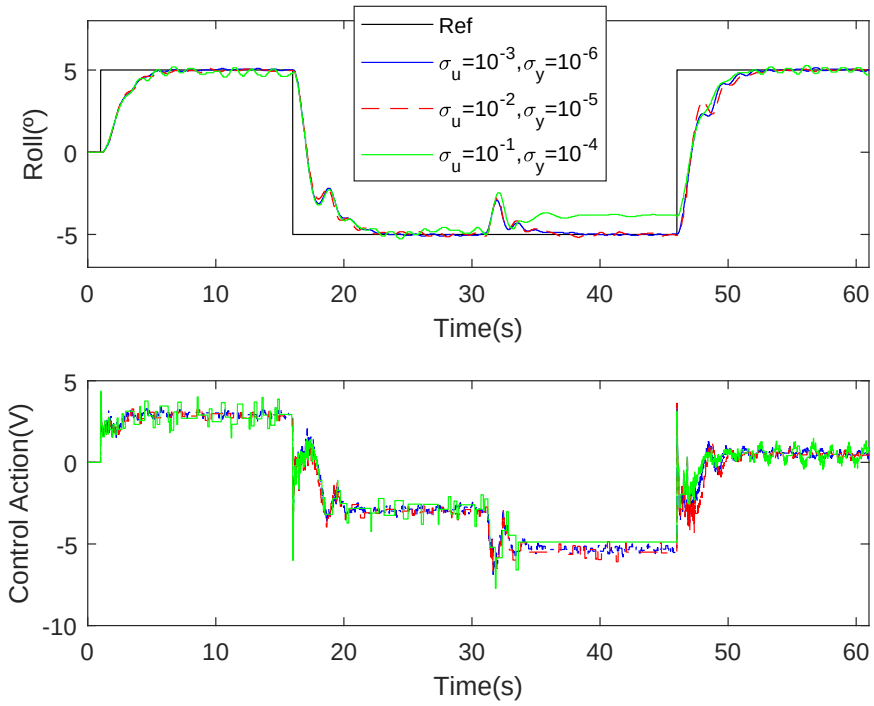

Figure 10: Experiment 2: Comparative of different values of σ_y and σ_u.

σ_u	σ_y	$SC(\%)$	$CA(\%)$
0.001	10^{-6}	**10.33%**	**35.88%**
0.01	10^{-5}	**10.16%**	**17.72%**
0.1	10^{-4}	**10.02%**	**12.11%**

Table 5: (Experimental setup) Comparison of the percentage of transmitted packets in both channels (columns $SC(\%)$ and $CA(\%)$)

8. Conclusions

In this paper, a novel control strategy for NCS, composed of a predictor-feedback scheme, event-triggered control and a gain-scheduled ESO, has been presented. Time-varying delays, packet loss and packet disorder in both links are counteracted, while the presence of mismatched disturbances is steady-state rejected. Furthermore, a control synthesis algorithm based on CCL and LMI has been provided in order to co-design the controller and event-triggered parameters in the aim of improving system performance. The benefits of our proposal are illustrated, that is, both communication problems and mismatched disturbances slightly affect the NCS, since it is able to keep satisfactory control properties despite reducing resource usage. Finally, the control solution is experimentally validated in a test-bed platform based on an unstable plant such as an Unmanned Aerial Vehicle (UAV).

Appendix A: Proof of Lemma 1

let us define $S = X^T X$, and consider the $\mathcal{L}_2$ norm of $w_{d,k}$ and $u_{d,k}$:

$$||w_d||_{l_2} = \left(\sum_{j=0}^{\infty} w_{d,j}^T S w_{d,j}\right)^{\frac{1}{2}}, \quad ||u_d||_{l_2} = \left(\sum_{j=0}^{\infty} u_{d,j}^T S u_{d,j}\right)^{\frac{1}{2}}. \tag{41}$$

Applying Jensen's inequality and replacing $w_{d,j} = \frac{1}{\tau_{CA}} \sum_{i=j-h_2^{CA}}^{j-h_1^{CA}-1} \phi(i) u_{d,i}$ into $||w_d||_{l_2}$ we have that:

$$\begin{aligned} ||w_d||_{l_2}^2 &= \frac{1}{\tau_{CA}^2} \sum_{j=0}^{\infty} \left(\sum_{i=j-h_2^{CA}}^{j-h_1^{CA}-1} \phi(i) u_{d,i}\right)^T S \left(\sum_{i=j-h_2^{CA}}^{j-h_1^{CA}-1} \phi(i) u_{d,i}\right) \\ &\leq \frac{1}{\tau_{CA}} \sum_{j=0}^{\infty} \sum_{i=j-h_2^{CA}}^{j-h_1^{CA}-1} \phi^2(i) u_{d,i}^T S u_{d,i} = \frac{1}{\tau_{CA}} \sum_{i=j-h_2^{CA}}^{j-h_1^{CA}-1} \underbrace{\sum_{j=0}^{\infty} u_{d,i}^T S u_{d,i}}_{||u_d||_{l_2}^2}. \end{aligned} \tag{42}$$

Then, we have that $||w_d||_{l_2}^2 \leq ||u_d||_{l_2}^2$ for any invertible matrix X, concluding the proof.

Appendix B: Proof of Theorem 2

Let $\bar{x}_k^T = \begin{bmatrix} x_k^T & \omega_k^T \end{bmatrix}$. From (3), system (1) with $\omega_{u,k} = 0$ can be expressed using the augmented state-space model:

$$\bar{x}_{k+1} = \mathcal{A}\bar{x}_k + \mathcal{B}u_{k-d_k^{CA}}, \tag{43}$$

where $\mathcal{A}$ and $\mathcal{B}$ are respectively defined in (4) and (21). Then, we have the following h-step ahead state prediction of $\bar{x}_k$:

$$\bar{x}_{k+h} = \mathcal{A}^h\bar{x}_k + \bar{\Omega}_{k+h}(h), \tag{44}$$

where

$$\bar{\Omega}_k(h) = \sum_{i=0}^{h-1} \mathcal{A}^{h-i-1}\mathcal{B}u_{k-h+i-d_{k-h+i}^{CA}}. \tag{45}$$

From the definition of $\mathcal{A}$ and $\mathcal{B}$ in (4) and (43) respectively, it can be deduced that $\bar{\Omega}_{k+h}(h) = \begin{bmatrix} \Omega_{k+h}^T(h) & 0_{m\times q} \end{bmatrix}^T$, where

$$\Omega_k(h) = \sum_{i=0}^{h-1} A^{h-i-1}Bu_{k-h+i-d_{k-h+i}^{CA}}. \tag{46}$$

The h-step back of (44) yields:

$$\bar{x}_k = \mathcal{A}^h\bar{x}_{k-h} + \bar{\Omega}_k(h). \tag{47}$$

Multiplying both-sides of (47) by $\mathcal{C}\mathcal{A}^{-h}$ we obtain:

$$\mathcal{C}\mathcal{A}^{-h}\bar{x}_k = \mathcal{C}\bar{x}_{k-h} + \mathcal{C}\mathcal{A}^{-h}\bar{\Omega}_k(h). \tag{48}$$

From the definition of $\mathcal{A}$, $\mathcal{C}$ in (4), we obtain that (48) is equivalent to:

$$\mathcal{C}\mathcal{A}^{-h}\bar{x}_k = Cx_{k-h} + CA^{-h}\Omega_k(h). \tag{49}$$

Replacing h by d_k^{SC} in the above expression we have:

$$\mathcal{C}\mathcal{A}^{-d_k^{SC}}\bar{x}_k = \underbrace{Cx_{k-d_k^{SC}}}_{\tilde{y}_{k-d_k^{SC}}} + CA^{-d_k^{SC}}\Omega_k(d_k^{SC}), \tag{50}$$

which leads to:

$$\tilde{y}_{k-ad_k^{SC}} = \mathcal{C}\mathcal{A}^{-d_k^{SC}}\bar{x}_k - CA^{-d_k^{SC}}\Omega_k(d_k^{SC}). \tag{51}$$

On the other hand, from (14), and defining

$$\rho_k = \frac{1}{\sqrt{\sigma_y}}\left(y_k - \tilde{y}_k\right), \tag{52}$$

we obtain:

$$\begin{aligned}\hat{\bar{z}}_{k+1} &= \mathcal{A}\hat{\bar{z}}_k + \tilde{\mathcal{B}}u_k + \mathcal{A}^{d_k^{SC}}\mathcal{L}\tilde{y}_{k-d_k^{SC}} + \sqrt{\sigma_y}\mathcal{A}^{d_k^{SC}}\mathcal{L}\rho_{k-d_k^{SC}} \\ &+ \mathcal{A}^{d_k^{SC}}\mathcal{L}CA^{-d_k^{SC}}\left(\Phi_k(h_1^{CA}) + \Phi_k(h_2^{CA}) + \Omega_k(d_k^{SC})\right) \\ &- \mathcal{A}^{d_k^{SC}}\mathcal{L}\mathcal{C}\mathcal{A}^{-d_k^{SC}}\hat{\bar{z}}_k.\end{aligned} \tag{53}$$

Substituting the term $\tilde{y}_{k-d_k^{SC}}$ from (51) into the above expression (53) and rearranging terms, we have:

$$\begin{aligned}\hat{\bar{z}}_{k+1} &= \mathcal{A}\hat{\bar{z}}_k + \tilde{\mathcal{B}}u_k \\ &+ \mathcal{A}^{d_k^{SC}}\mathcal{L}CA^{-d_k^{SC}}\left(\Phi_k(h_1^{CA}) + \Phi_k(h_2^{CA})\right) \\ &+ \mathcal{A}^{d_k^{SC}}\mathcal{L}\mathcal{C}\mathcal{A}^{-d_k^{SC}}\left(\bar{x}_k - \hat{\bar{z}}_k\right) + \sqrt{\sigma_y}\mathcal{A}^{d_k^{SC}}\mathcal{L}\rho_{k-d_k^{SC}}.\end{aligned} \tag{54}$$

Noting that $\bar{x}_k^T = \left(x_k^T,\ \omega_k^T\right)$ and $x_k = z_k - \Phi_k(h_1^{CA}) - \Phi_k(h_2^{CA})$ (see (12)) it can be deduced that $\bar{x}_k = \bar{z}_k - \bar{\Phi}_k(h_1^{CA}) - \bar{\Phi}_k(h_2^{CA})$, where $\bar{\Phi}_k(h_i^{CA}) = \begin{bmatrix}\Phi_k^T(h_i^{CA}) & 0_{m\times q}\end{bmatrix}^T$ $i = 1, 2$ and $\bar{z}_k^T = [z_k^T,\ \ \omega_k^T]$. Then, replacing $\bar{x}_k$ by $\bar{z}_k - \bar{\Phi}_k(h_1^{CA}) - \bar{\Phi}_k(h_2^{CA})$ into (54), and taking into account that $\mathcal{C}\mathcal{A}^{-d_k^{SC}}\bar{\Phi}_k(h_i^{CA}) = CA^{-d_k^{SC}}\Phi_k(h_i^{CA})$, $i = 1, 2$, we obtain:

$$\begin{aligned}\hat{\bar{z}}_{k+1} &= \mathcal{A}\hat{\bar{z}}_k + \tilde{\mathcal{B}}u_k + \mathcal{A}^{d_k^{SC}}\mathcal{L}\mathcal{C}\mathcal{A}^{-d_k^{SC}}\left(\bar{z}_k - \hat{\bar{z}}_k\right) \\ &+ \sqrt{\sigma_y}\mathcal{A}^{d_k^{SC}}\mathcal{L}\rho_{k-d_k^{SC}}.\end{aligned} \tag{55}$$

Let $\bar{e}_k = \bar{z}_k - \hat{\bar{z}}_k$. Then, we can write $\tilde{u}_k = \mathcal{K}\hat{\bar{z}}_k$ as:

$$\tilde{u}_k = \mathcal{K}\bar{z}_k - \mathcal{K}\bar{e}_k \tag{56}$$

The one-step ahead z_{k+1} and $\bar{e}_{k+1}$ yield:

$$\begin{aligned}z_{k+1} &= Az_k + \tilde{B}\left(\tilde{u}_k + \sqrt{\sigma_u}\eta_k\right) + Gw_{d,k} + Fw_k, \\ \bar{e}_{k+1} &= \left(\mathcal{A} - \mathcal{A}^{d_k^{SC}}\mathcal{L}\mathcal{C}\mathcal{A}^{-d_k^{SC}}\right)\bar{e}_k \\ &+ \mathcal{G}w_{d,k} - \sqrt{\sigma_y}\mathcal{A}^{d_k^{SC}}\mathcal{L}\rho_{k-d_k^{SC}}\end{aligned} \tag{57}$$

where

$$\eta_k = \frac{1}{\sqrt{\sigma_u}} \left(u_k - \tilde{u}_k \right). \tag{58}$$

Taking into account the above expressions, the augmented state-space model renders:

$$\begin{aligned} \begin{bmatrix} z_{k+1} \\ u_k \\ \bar{e}_{k+1} \end{bmatrix} &= \begin{bmatrix} A + \tilde{B}K_z & 0 & -\tilde{B}\mathcal{K} \\ K_z & 0 & -\mathcal{K} \\ 0 & 0 & \mathcal{A} - \mathcal{A}^{d_k^{SC}} \mathcal{L}\mathcal{C}\mathcal{A}^{-d_k^{SC}} \end{bmatrix} \begin{bmatrix} z_k \\ u_{k-1} \\ \bar{e}_k \end{bmatrix} \\ &+ \begin{bmatrix} G \\ 0 \\ \mathcal{G} \end{bmatrix} w_{d,k} + \begin{bmatrix} \sqrt{\sigma_u}\tilde{B} \\ 0 \\ 0 \end{bmatrix} \eta_k - \begin{bmatrix} 0 \\ 0 \\ (\tau_{SC}+1)\sqrt{\sigma_y}\mathcal{A}^{d_k^{SC}} \mathcal{L} \end{bmatrix} \tilde{\rho}_k \\ &+ \begin{bmatrix} F + \tilde{B}K_w \\ K_w \\ 0 \end{bmatrix} w_k, \end{aligned} \tag{59}$$

where $\tilde{\rho}_k = \left(\frac{1}{\tau_{SC}+1} \right) \rho_{k-d_k^{SC}}$.

From (8), (9), (18), and (19), it can be deduced that the following conditions always hold:

$$\begin{aligned} \left(u_k - \tilde{u}_k \right)^T \Omega_u \left(u_k - \tilde{u}_k \right) &\leq \sigma_u \tilde{u}_k^T \Omega_u \tilde{u}_k, \\ \left(y_k - \tilde{y}_k \right)^T \Omega_y \left(y_k - \tilde{y}_k \right) &\leq \sigma_y \tilde{y}_k^T \Omega_y \tilde{y}_k, \end{aligned} \tag{60}$$

From (52) and (58), the above expressions can be equivalently written as:

$$\eta_k = \Delta_{\eta,k} \tilde{u}_k, \qquad \rho_k = \Delta_{\rho,k} \tilde{y}_k \tag{61}$$

where $\Delta_\eta : \tilde{u} \to \eta$ and $\Delta_\rho : \tilde{y} \to \rho$ are time-varying operators satisfying respectively:

$$||X_u \Delta_\eta X_u^{-1}||_\infty \leq 1, \qquad ||X_y \Delta_\rho X_y^{-1}||_\infty \leq 1 \tag{62}$$

where $X_u^T X_u = \Omega_u$ and $X_y^T X_y = \Omega_y$. Together with $\Delta_d : \ u_d \to w_d$ (already defined in Lemma 1), and the above defined Δ_η, Δ_ρ, the following normalized time-varying delay operator $\Delta_{\rho,d}$ is also introduced:

$$\begin{aligned} &\Delta_{\rho,d} : \ \rho \to \tilde{\rho}, \\ &\Delta_\rho^* = \Delta_\rho \, \Delta_{\rho,d} : \ \tilde{y} \to \tilde{\rho}, \end{aligned} \tag{63}$$

where $\tilde{\rho}_k = \Delta^*_{\rho,k}\rho_k = \left(\frac{1}{\tau_{SC}+1}\right)\rho_{k-d_k^{SC}}$. Noting that $||\Delta_\rho||_\infty \leq 1$, $||\Delta_{\rho,d}||_\infty \leq 1$, we have that $||\Delta^*_\rho||_\infty \leq 1$. Therefore, from Lemma 1 and (61), we have that:

$$\begin{bmatrix} w_{d,k} \\ \eta_k \\ \tilde{\rho}_k \end{bmatrix} = \begin{bmatrix} \Delta_d & 0 & 0 \\ 0 & \Delta_\eta & 0 \\ 0 & 0 & \Delta^*_\rho \end{bmatrix} \begin{bmatrix} u_{d,k} \\ \tilde{u}_k \\ \tilde{y}_k \end{bmatrix}, \tag{64}$$

where

$$\begin{aligned} u_{d,k} &= u_k - u_{k-1} \\ &= \begin{bmatrix} K_z & -I_m & -\mathcal{K} \end{bmatrix} \xi_k + \sqrt{\sigma_u}\eta_k + K_w w_k, \\ \tilde{u}_k &= \mathcal{K}\left(\bar{z}_k - \bar{e}_k\right) = \begin{bmatrix} K_z & 0 & -\mathcal{K} \end{bmatrix} \xi_k + K_w w_k, \\ \tilde{y}_k &= Cx_k = Cz_k - C\left(\Phi_k(h_1^{CA}) + \Phi_k(h_2^{CA})\right) \end{aligned} \tag{65}$$

Note that the following equivalence is satisfied:

$$\Phi_k(h_1^{CA}) + \Phi_k(h_2^{CA}) = \Gamma_1 u_{k-1} - \Pi_k \tag{66}$$

where Γ_1 is defined in (24), and

$$\begin{aligned} \Pi_k = &\sum_{j=0}^{h_1^{CA}-1} \sum_{f=1}^{h_1^{CA}-j-1} A^{-j-1}\frac{B}{2}u_{d,k-f} \\ &+ \sum_{j=0}^{h_2^{CA}-1} \sum_{f=1}^{h_2^{CA}-j-1} A^{-j-1}\frac{B}{2}u_{d,k-f} \end{aligned} \tag{67}$$

Also, with the above notation, the output $\tilde{y}_k$ in (65) can be expressed as:

$$\tilde{y}_k = \begin{bmatrix} C & C\Gamma_1 & 0 \end{bmatrix} \xi_k - \mu C \nu_k, \qquad \nu_k = \Delta_\nu u_{d,k}, \tag{68}$$

where $\xi_k^T = \begin{bmatrix} z_k^T & u_{k-1}^T & \bar{e}_k^T \end{bmatrix}$, and the scalar μ is the H_∞ norm of the operator $\Pi_k : u_d \to \nu$, which is defined in (24).

Next, let us introduce the vectors:

$$\begin{aligned} \bar{w}_k^T &= \begin{bmatrix} w_{d,k}^T & \eta_k^T & \tilde{\rho}_k^T & \nu_k^T \end{bmatrix}, \\ \bar{y}_k^T &= \begin{bmatrix} u_{d,k}^T & \tilde{u}_k^T & \tilde{y}_k^T & u_{d,k}^T \end{bmatrix} \end{aligned} \tag{69}$$

From the above definitions and (64), we can write:

$$\bar{w}_k = \bar{\Delta}\bar{y}_k, \qquad \bar{\Delta} = diag\left(\Delta_d,\ \Delta_\eta,\ \Delta^*_\rho,\ \Delta_\nu\right). \tag{70}$$

Note from the structure of $\bar{\Delta}$ in (70) that $T_2\bar{\Delta} = \bar{\Delta}T_1$, where T_1, T_2 are defined in (23), and therefore $||T_1\bar{\Delta}T_2^{-1}||_\infty \leq 1$. Finally, from (70), the interconnected system (22) is obtained, concluding the proof.

Appendix C: Proof of Theorem 1

Consider the Lyapunov function $V_k = \xi_k^T P^{-1} \xi_k$, where $P > 0$ and ξ_k^T defined in (22). The system M_S in (22) is asymptotically stable with decay rate β, say $||\xi_k|| \leq \Omega ||\xi_0||^{-\beta}, \forall k \geq 0$, for some arbitrary $\Omega > 0$ and any initial condition ξ_0, if the following condition holds:

$$\Delta_\beta V_k = V_{k+1} - \beta^2 V_k < 0. \tag{71}$$

On the other hand, note that the controlled output $y_{s,k}$ in (1) renders:

$$y_{s,k} = \bar{C}_s \xi_k + \bar{D}_s \bar{w}_k, \tag{72}$$

where $\bar{C}_s$ and$\bar{D}_s$ are defined in (27).

It is well-known that the following condition along (M_S):

$$\Delta_\beta V_k + \bar{y}_k^T \mathcal{W}_2^{-1} \bar{y}_k - \bar{w}_k^T \mathcal{W}_1^{-1} \bar{w}_k + y_{s,k}^T y_{s,k} - \gamma^2 w_k^T w_k < 0, \tag{73}$$

implies that $||T_2 M_S T_1^{-1}||_\infty \leq 1$ and $||y_s||^2 \leq \gamma^2 ||\bar{w}||^2$, where T_1, T_2 are defined in (23) and $\mathcal{W}_1^{-1} = T_1^T T_1$, $\mathcal{W}_2^{-1} = T_2^T T_2$.

From (22) and (72), the expression (73) yields:

$$\begin{aligned} &\xi_k^T \left(\bar{A}_k^T P^{-1} \bar{A}_k - \beta^2 P^{-1} + \bar{H}^T \mathcal{W}_2^{-1} \bar{H} + \bar{C}_s^T \bar{C}_s \right) \xi_k \\ &+ 2\xi_k^T \bar{A}_k^T P \bar{G}_k \bar{w}_k + 2\xi_k^T \bar{C}_s^T \bar{D}_s w_k \\ &+ 2\xi_k^T \bar{A}_k^T P \bar{F} w_k + \bar{w}_k^T \left(\bar{G}_k^T P \bar{G}_k - \mathcal{W}_1^{-1} \right) \bar{w}_k \\ &+ 2\bar{w}_k^T \bar{G}_k^T P \bar{F} w_k + w_k^T \left(\bar{D}_s^T \bar{D}_s - \gamma^2 I_q \right) w_k < 0. \end{aligned} \tag{74}$$

Applying Schur Complement, the following inequality is obtained:

$$\hat{\Gamma}_i = \begin{bmatrix} -\beta^2 P^{-1} & 0 & 0 & \hat{\bar{A}}_i^T & \bar{H}^T & \bar{C}_s^T \\ (*) & -\mathcal{W}_1^{-1} & 0 & \hat{\bar{G}}_i^T & \bar{D}^T & \bar{D}_s^T \\ (*) & (*) & -\gamma^2 I_q & \bar{F}^T & \bar{J}^T & 0 \\ (*) & (*) & (*) & -P & 0 & 0 \\ (*) & (*) & (*) & (*) & -\mathcal{W}_2 & 0 \\ (*) & (*) & (*) & (*) & (*) & -I_{p_s} \end{bmatrix}. \tag{75}$$

Pre-and post multiplying the above inequality by

$$diag\,(P, \quad \mathcal{W}_1, \quad I, \quad I, \quad I, \quad I), \tag{76}$$

and writing

$$\left(\bar{A}_k, \bar{G}_k\right) = \sum_{i=1}^{r} \lambda_i(d_k^{SC}) \left(\hat{\bar{A}}_i, \hat{\bar{G}}_i\right), \tag{77}$$

where $r = h_2^{SC} - h_1^{SC} + 1$, being $\hat{\bar{A}}_i$, $\hat{\bar{G}}_i$ is defined in (27), and

$$\lambda_i(d_k^{SC}) = \begin{cases} 1 & \text{if } d_k^{SC} - h_1^{SC} + 1 = i \\ 0 & \text{otherwise,} \end{cases} \tag{78}$$

the inequality (74) is equivalent to:

$$\sum_{i=1}^{r} \lambda_i(d_k^{SC}) \tilde{\Gamma}_i < 0, \tag{79}$$

where $\tilde{\Gamma}_i$ is defined in (26). Taking into account that the scalar functions $\lambda_i(.)$ in (78) satisfy the convex sum properties: $\sum_{i=1}^{r} \lambda_i(.) = 1, \quad 0 \leq \lambda_i(.) \leq 1$, a sufficient condition for (79) is given in (25).

References

[1] Z. Artstein. Linear systems with delayed controls: a reduction. *IEEE Transactions on Automatic control*, 27(4):869–879, 1982.

[2] A. Baños, F. Perez, and J. Cervera. Network-based reset control systems with time-varying delays. *IEEE Transactions on Industrial Informatics*, 10(1):514–522, 2014.

[3] A. Castillo, P. García, R. Sanz, and P. Albertos. Enhanced extended state observer-based control for systems with mismatched uncertainties and disturbances. *ISA transactions*, 2017.

[4] M. B. Cloosterman, N. Van de Wouw, W. Heemels, and H. Nijmeijer. Stability of networked control systems with uncertain time-varying delays. *IEEE Transactions on Automatic Control*, 54(7):1575–1580, 2009.

[5] A. Cuenca, P. García, P. Albertos, and J. Salt. A non-uniform predictor-observer for a networked control system. *International Journal of Control, Automation and Systems*, 9(6):1194–1202, 2011.

[6] A. Cuenca, J. Alcaina, J. Salt, V. Casanova, and R. Pizá. A packet-based dual-rate pid control strategy for a slow-rate sensing networked control system. *ISA transactions*, 76:155–166, 2018.

[7] A. Cuenca, D. Antunes, A. Castillo, P. García, B. A. Khashooei, and W. Heemels. Periodic event-triggered sampling and dual-rate control for a wireless networked control system with applications to UAVs. *IEEE Transactions on Industrial Electronics*, 66(4):3157–3166, 2018.

[8] A. Cuenca, M. Zheng, M. Tomizuka, and S. Sánchez. Non-uniform multi-rate estimator based periodic event-triggered control for resource saving. *Information Sciences*, 459:86–102, 2018.

[9] D. Dolz, I. Peñarrocha, and R. Sanchis. Networked gain-scheduled fault diagnosis under control input dropouts without data delivery acknowledgment. *International Journal of Robust and Nonlinear Control*, 26(4): 737–758, 2016.

[10] L. El Ghaoui, F. Oustry, and M. AitRami. A cone complementarity linearization algorithm for static output-feedback and related problems. *IEEE transactions on automatic control*, 42(8):1171–1176, 1997.

[11] E. Garone, A. Gasparri, and F. Lamonaca. Clock synchronization protocol for wireless sensor networks with bounded communication delays. *Automatica*, 59:60–72, 2015.

[12] X. Ge and Q.-L. Han. Distributed formation control of networked multi-agent systems using a dynamic event-triggered communication mechanism. *IEEE Transactions on Industrial Electronics*, 64(10):8118–8127, 2017.

[13] A. González, A. Sala, and R. Sanchis. LK stability analysis of predictor-based controllers for discrete-time systems with time-varying actuator delay. *Systems & Control Letters*, 62(9):764–769, 2013.

[14] A. González, V. Balaguer, P. G. Gil, and A. Cuenca. Gain-scheduled predictive extended state observer for time-varying delays systems with mismatched disturbances. *ISA transactions*, 2018.

[15] R. A. Gupta and M. Y. Chow. Networked control system: overview and research trends. *IEEE Transactions on Industrial Electronics*, 57 (7):2527–2535, 2010.

[16] Y. Halevi and A. Ray. Integrated communication and control systems: Part i -analysis. *Journal of Dynamic Systems, Measurement, and Control*, 110(4):367–373, 1988.

[17] S. Hao, T. Liu, and B. Zhou. Predictor-based output feedback control design for sampled systems with input delay subject to disturbance. *IET Control Theory & Applications*, 11(18):3329–3340, 2017.

[18] W. Heemels and M. Donkers. Model-based periodic event-triggered control for linear systems. *Automatica*, 49(3):698–711, 2013.

[19] W. Heemels, M. Donkers, and A. R. Teel. Periodic event-triggered control for linear systems. *IEEE Transactions on Automatic Control*, 58 (4):847–861, 2013.

[20] H. Li and Y. Shi. Network-based predictive control for constrained nonlinear systems with two-channel packet dropouts. *IEEE Transactions on Industrial Electronics*, 61(3):1574–1582, 2014.

[21] L.-W. Liou and A. Ray. Integrated communication and control systems: Part iii: Nonidentical sensor and controller sampling. *Journal of Dynamic Systems, Measurement, and Control*, 112(3):357–364, 1990.

[22] A. Liu, W. A. Zhang, L. Yu, S. Liu, and M. Z. Chen. New results on stabilization of networked control systems with packet disordering. *Automatica*, 52:255–259, 2015.

[23] A. Liu, W. A. Zhang, B. Chen, and L. Yu. Networked filtering with markov transmission delays and packet disordering. *IET Control Theory & Applications*, 12(5):687–693, 2017.

[24] D. Liu and G. H. Yang. Robust event-triggered control for networked control systems. *Information Sciences*, 459:186–197, 2018.

[25] T. Liu, S. Hao, D. Li, W. H. Chen, and Q. G. Wang. Predictor-based disturbance rejection control for sampled systems with input delay. *IEEE Transactions on Control Systems Technology*, 2017.

[26] X. Luan, P. Shi, and F. Liu. Stabilization of networked control systems with random delays. *IEEE Transactions on Industrial Electronics*, 58 (9):4323–4330, 2011.

[27] J. Lunze and D. Lehmann. A state-feedback approach to event-based control. *Automatica*, 46(1):211–215, 2010.

[28] M. Mazo and P. Tabuada. On event-triggered and self-triggered control over sensor/actuator networks. In *Decision and Control, 2008. CDC 2008. 47th IEEE Conference on*, pages 435–440. IEEE, 2008.

[29] J. E. Normey-Rico. *Control of dead-time processes*. Springer Science & Business Media, 2007.

[30] I. Peñarrocha, R. Sanchis, and J. A. Romero. State estimator for multi-sensor systems with irregular sampling and time-varying delays. *International Journal of Systems Science*, 43(8):1441–1453, 2012.

[31] F. Perez, A. Baños, and J. Cervera. Design of networked reset control systems for reference tracking. In *IECON 2011-37th Annual Conference on IEEE Industrial Electronics Society*, pages 2566–2571. IEEE, 2011.

[32] A. Ray and Y. Halevi. Integrated communication and control systems: Part ii -design considerations. *Journal of Dynamic Systems, Measurement, and Control*, 110(4):374–381, 1988.

[33] A. Sala, A. Cuenca, and J. Salt. A retunable PID multi-rate controller for a networked control system. *Information Sciences*, 179(14):2390–2402, 2009.

[34] R. Sanz, P. García, and P. Albertos. Enhanced disturbance rejection for a predictor-based control of lti systems with input delay. *Automatica*, 72:205–208, 2016.

[35] R. Sanz, P. García, Q. Zhong, and P. Albertos. Predictor-based control of a class of time-delay systems and its application to quadrotors. *IEEE Transactions on Industrial Electronics*, 64(1):459–469, 2017.

[36] R. Sanz, P. Garcia, E. Fridman, and P. Albertos. Rejection of mismatched disturbances for systems with input delay via a predictive extended state observer. *International Journal of Robust and Nonlinear Control*, 28(6):2457–2467, 2018.

[37] W. Wu and Y. Zhang. Event-triggered fault-tolerant control and scheduling codesign for nonlinear networked control systems with medium-access constraint and packet disordering. *International Journal of Robust and Nonlinear Control*, 28(4):1182–1198, 2018.

[38] R. Yang, G. P. Liu, P. Shi, C. Thomas, and M. V. Basin. Predictive output feedback control for networked control systems. *IEEE Transactions on Industrial Electronics*, 61(1):512–520, 2014.

[39] T. C. Yang. Networked control system: a brief survey. *IEE Proceedings Control Theory and Applications*, 153(4):403, 2006.

[40] D. Zhang, P. Shi, Q. G. Wang, and L. Yu. Analysis and synthesis of networked control systems: a survey of recent advances and challenges. *ISA Transactions*, 66:376–392, 2017.

[41] J. Zhang, J. Lam, and Y. Xia. Output feedback delay compensation control for networked control systems with random delays. *Information Sciences*, 265:154–166, 2014.

[42] J. Zhang, Y. Lin, and P. Shi. Output tracking control of networked control systems via delay compensation controllers. *Automatica*, 57: 85–92, 2015.

[43] L. Zhao, H. Gao, and P. Shi. Stability and stabilization of TS fuzzy systems with time-varying delay: An input-output approach. In *50th IEEE Conference on Decision and Control and European Control Conference (CDC-ECC), 2011*, pages 8285–8290. IEEE, 2011.

[44] W. Zou and Z. Xiang. Event-triggered containment control of second-order nonlinear multi-agent systems. *Journal of the Franklin Institute*, 2018.

[45] W. Zou and Z. Xiang. Event-triggered leader–following consensus of non-linear multi-agent systems with switched dynamics. *IET Control Theory & Applications*, 2018.